PROGRESS IN COLOR, COLORANTS AND COATINGS

available online @ www.pccc.icrc.ac.ir

Progress in Color Colorants Coating 20 (2027), 367-389

Ministry of Science, Research and Technology
Institute for Color Science & Technology

HBAT as a High-Efficiency Corrosion Inhibitor for Mild Steel in 1 M HCl: Gravimetric, Electrochemical, Adsorption, and Surface Studies

R. Khalid Ahmed[1], H. Saad Azeez[2], R. J. Halbos[3], A. Amir H. Kadhum[4], A. Al-Amiery[3, 5*]

[1.] Department of Petroleum and Gas Refining Engineering, College of Petroleum Processes Engineering, Tikrit University, P.O. Box: 34001, Saladin, Iraq

[2.] College of Civil Engineering, University of Technology-Iraq, P.O. Box: 10066, Baghdad, Iraq

[3.] Energy and Renewable Energies Technology Center, University of Technology-Iraq, P.O. Box:10066, Baghdad, Iraq

[4.] Faculty of Medicine, University of Al-Ameed, P.O. Box: 56001, Karbala, Iraq

[5.] Department of Sciences and Technology Parks, Al-Ayen Iraqi University, AUIQ, An Nasiriyah, P.O. Box: 64004, Thi Qar, Iraq

ARTICLE INFO

Article history:
Received: 03 Aug 2026
Final Revised: 16 Nov 2025
Accepted: 20 Nov 2025
Available online: 16 Nov 2026

Keywords:
Mild steel
Corrosion inhibition
Aminothiazole
Electrochemical impedance
Langmuir isotherm

ABSTRACT

N-(2-hydroxybenzoyl)-2-aminothiazole (HBAT) was evaluated as a corrosion inhibitor for mild steel in 1 M HCl by weight loss, electrochemical impedance spectroscopy (EIS), adsorption analysis, and scanning electron microscopy (SEM). Inhibition increased with HBAT concentration and immersion time, reaching 96.82 % at 0.5 mM after 24 h at 303 K and remaining 96.81 % after 48 h. Increasing the concentration to 1.0 mM produced only a marginal additional improvement, indicating a practical plateau near 0.5 mM. At 0.5 mM, inhibition increased to 96.65 % at 333 K. EIS at 303 K showed a marked increase in charge-transfer resistance and an inhibition efficiency of 94.91 % at 0.5 mM. Adsorption was best described by the Langmuir isotherm, and SEM showed reduced surface damage. The inhibition mechanism is proposed to involve mixed physical and chemical adsorption, likely through electrostatic interactions and electron donation from heteroatoms (N, S, O) and the aromatic π-system to the steel surface. These findings identify HBAT as a highly efficient inhibitor under the investigated conditions. Prog Color Colorants Coat. 20 (2027), 367-389© Institute for Color Science and Technology.

1. Introduction

Its low cost, ready availability, useful mechanical properties, and ease of fabrication make mild steel common in pipelines, storage vessels, heat-transfer equipment, construction, and chemical-processing facilities. A major limitation, however, is its rapid deterioration in acidic media. Industry uses hydrochloric acid for pickling, cleaning, scale removal, removal of corrosion deposits, and well acidizing [1-3]. When unprotected steel contacts this medium, iron oxidation and hydrogen evolution accelerate, leading to material loss, reduced structural integrity, product contamination, and higher maintenance expenditure. Several approaches, including metallic and organic coatings, cathodic protection, alloy modification, and the use of corrosion-resistant materials, have been developed to control metallic corrosion. Among the available control strategies, dosing the acid with a small amount of inhibitor is often the least disruptive and most economical option [4, 5]. Adsorbed inhibitor molecules cover reactive regions of the steel and limit the approach of H^+, Cl^-, and water to the metal surface. Iron corrosion can be slowed when inhibitors change what happens at the metal surface. Some stop

*Corresponding author: * dr.ahmed1975@gukm.edu.my
dr.ahmed1975@gmail.com

https://doi.org/10.30509/pccc.2026.167849.1528

the anodic iron loss, some slow the cathodic hydrogen forming step, and some reduce both at once [6, 7]. In acid solutions, organic inhibitors tend to work well when they have conjugated rings and include N, S, or O atoms. These groups can offer lone pairs and spread out π electrons, which helps them interact with iron on the surface [8, 9]. Many details decide how well an inhibitor performs. Things like the molecule size, how flat it is, the electron strength, its solubility, how it behaves in the presence of protons, and what its substituents do all matter. The number of adsorption sites and how easy they are to reach also play a key role. In hydrochloric acid, the story can shift with protonation. Protonated inhibitor molecules can be pulled toward areas that have chloride at the interface. Meanwhile, neutral or only slightly protonated species may attach by using lone pairs or π electrons. There can also be extra stabilization from electron back-donation from iron to the inhibitor [10]. The final result is a mix of electrostatic effects and chemical bonding. That mix depends on the inhibitor structure and on the test conditions [11].

Heterocyclic compounds are particularly promising because their rings provide well-defined adsorption centers and frequently exhibit good stability under strongly acidic conditions. Oxazole, isoxazole, thiazole, thiadiazole, benzoxazole, benzimidazole, triazole, and phenanthroline derivatives have therefore been investigated for the protection of steels in acidic media [1, 4-8]. For example, an isoxazole derivative provided more than 90 % protection for mild steel in 1 M HCl under optimized conditions [6], whereas benzoxazole-2-thione reached an inhibition efficiency of 95.25 % at a concentration of 10^{-4} M [7]. A benzimidazole-thiophene ligand and its metal complexes also substantially reduced the corrosion current density of mild steel in 1 M HCl, with the zinc complex producing an inhibition efficiency of 93.8% [4]. These studies associated the improved protection with strong molecular adsorption, increased charge-transfer resistance, decreased double-layer capacitance, and the formation of compact protective films on the steel surface. Sulfur- and nitrogen-containing azoles are especially relevant to the development of efficient corrosion inhibitors. Thiadiazole derivatives have been shown to inhibit mild-steel dissolution by blocking interfacial charge- and mass-transfer processes [5, 12, 13]. Their inhibition efficiency is commonly attributed to adsorption through sulfur and nitrogen atoms, together with the contribution of aromatic or conjugated substituents. Related oxadiazole derivatives have also demonstrated effective inhibition in hydrochloric acid by increasing interfacial resistance and reducing the fraction of the steel surface exposed to the corrosive solution [14]. Adding more donor groups and aromatic parts to an azole-like molecular core can raise the count of adsorption contacts. It can also help the surface coverage go up. HBAT stands out for corrosion control. It has a thiazole ring plus an aromatic hydroxybenzamide piece. In the thiazole ring there are sulfur and nitrogen atoms. The structure also includes an amide carbonyl group and an amide nitrogen. There is a phenolic hydroxyl group too. On top of that, the molecule has an aromatic pi electron system. Because of these parts, there are many spots where the molecule can bind to mild steel. The thiazole sulfur and the thiazole nitrogen can take part in coordination with iron on the surface. The carbonyl oxygen can also help through donor acceptor type contact. The aromatic ring can support coverage through pi metal interactions. The ortho hydroxyl group can shift how charge sits on the molecule. It can also change how the molecule meets the interface. Results that others reported for similar thiadiazole compounds support this direction. The same is true for 2-(2-hydroxyphenyl)benzothiazole. For that reason, it makes sense to test the mixed hydroxybenzoyl aminothiazole form [12, 13, 15]. HBAT was studied in a 1 M hydrochloric acid solution to determine its effectiveness as a multi-component corrosion inhibitor. HBAT contains several groups, including thiazol, amide, phenol, and aromatic units. Therefore, it can bind to metals at multiple sites. The idea is that these bonds work together, enabling HBAT to coat the surface effectively and form a thin, corrosion-resistant layer. Most previous reports focused on a single test setup. In this study, the effects of several experimental parameters, including inhibitor concentration, solution temperature, and immersion time, were systematically investigated to evaluate their influence on the corrosion-inhibition performance of HBAT. The inhibition behavior was assessed using complementary experimental techniques. Weight-loss measurements were employed to determine variations in the corrosion rate and inhibition efficiency under different experimental conditions, while electrochemical impe-dance spectroscopy (EIS) was used to characterize the interfacial processes occurring at the mild steel/

solution interface and to provide further insight into the formation and protective behavior of the adsorbed inhibitor layer. Adsorption isotherms were used to explain how HBAT molecules interact with the metal surface. Scanning electron microscopy was used to examine the protective layer and to assess the extent of acid damage to the surface after treatment. The primary objective was to evaluate the effectiveness of HBAT in preventing the corrosion of mild steel in a 1 M hydrochloric acid solution. The primary objective was to evaluate the corrosion-inhibition performance of HBAT for mild steel in 1 M HCl as a function of concentration, immersion time, and temperature. Weight-loss measurements provided corrosion rates and inhibition efficiencies. EIS was used to monitor changes in charge-transfer resistance and interfacial capacitance at 303 K. Adsorption isotherms and van 't Hoff analysis were used to describe the macroscopic adsorption behaviour. SEM was used to compare surface damage in the absence and presence of HBAT. A mixed physical and chemical adsorption mode is proposed on the basis of molecular structure, literature precedent, and DFT donor-site descriptors; it is not treated as a spectroscopically demonstrated mechanism.

2. Experimental

2.1. Materials and preparation of mild-steel specimens

Mild-steel samples came from Metal Samples Company. Their target chemistry was given in wt.%: C 0.210, Mn 0.050, Si 0.380, Al 0.010, S 0.050, P 0.090, and Fe for the rest. For weight loss and surface viewing, rectangular coupons were cut to 4.0 × 2.5 × 0.1 cm. For the electrochemical runs, smaller pieces were made, each at 1.0 × 1.0 × 0.1 cm. Right before any tests, the exposed faces were leveled by grinding. The order was 400 grit SiC, then 600 grit, then 1200 grit. Residual particles were removed with double-distilled water, after which the specimens were cleaned with ethanol and air-dried. This sequence was applied to every coupon to provide comparable starting surfaces [16]. The molecular structure of N-(2-hydroxybenzoyl)-2-aminothiazole, hereafter denoted as HBAT, is presented in Figure 1.

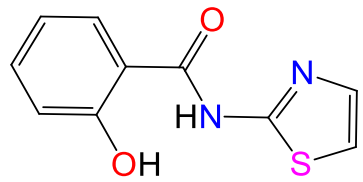


Figure 1: Molecular structure of HBAT.

2.2. Preparation of the corrosive and inhibited solutions

Analytical-grade HCl (37 %, Merck, Malaysia) was diluted with double-distilled water to prepare 1 M HCl. N-(2-hydroxybenzoyl)-2-aminothiazole (HBAT) was commercially obtained from Sigma-Aldrich, Selangor, Malaysia. Calculated quantities of HBAT were dissolved in the corrosive medium to prepare the required inhibitor concentrations, while freshly prepared 1 M HCl without HBAT served as the blank.

2.3. Gravimetric measurements

Gravimetric measurements were performed in accordance with the relevant NACE procedures [16, 17]. Each coupon was weighed before being fully submerged in blank or HBAT-containing 1 M HCl. Masses were recorded using a Precisa XB 220A analytical balance (Precisa Gravimetrics AG, Switzerland) with a precision of ±0.0001 g. Each gravimetric condition was measured in three independent replicates, and the reported corrosion rates and inhibition efficiencies are mean values. Temperature tests used a constant 5 h exposure between 303 and 333 K; separate time-series experiments at 303 K used immersion periods of 1, 5, 10, 24, and 48 h over the 0.1-0.5 mM concentration range. An additional concentration of 1.0 mM was examined gravimetrically at the same immersion periods to evaluate whether the inhibition efficiency continued to increase significantly beyond 0.5 mM. After the designated exposure period, the coupons were removed, cleaned to eliminate loosely adherent corrosion products, rinsed with double-distilled water, dried, and reweighed. The corrosion rate, C_R, expressed in mg cm^{-2} h^{-1}, was determined from the mass loss according to equation 1.

$$C_R = \frac{\Delta m}{At} \quad (1)$$

where Δm is the difference between the initial and final masses of the specimen, A is the total surface area exposed to the solution, and $t$is the immersion time.

The gravimetric inhibition efficiency, IE_{WL}, was calculated using equation 2.

$$IE_{WL}(\%) = \frac{C_R^0 - C_R^{inh}}{C_R^0} \times 100 \quad (2)$$

The corresponding fractional surface coverage, θ, was obtained from equation 3.

$$\theta = \frac{C_R^0 - C_R^{inh}}{C_R^0} \quad (3)$$

where C_R^0 and C_R^{inh} are the corrosion rates measured in the absence and presence of HBAT, respectively [18].

2.4. Adsorption isotherms

The adsorption behavior of HBAT at the mild-steel/ solution interface was examined using the surface-coverage values obtained from the gravimetric measurements. The experimental data were fitted to the Langmuir, Freundlich, Temkin, and Frumkin adsorption models. The quality of each fit was assessed from the corresponding linear-regression coefficient, slope, and agreement between the experimental and theoretical behavior. The linear form of the Langmuir adsorption isotherm is expressed as Eq. 4.

$$\frac{C_{inh}}{\theta} = \frac{1}{K_{ads}} + C_{inh} \quad (4)$$

where C_{inh} is the molar concentration of HBAT and K_{ads} is the adsorption–desorption equilibrium constant. A plot of C_{inh}/θ against C_{inh} should produce a straight line when the adsorption process obeys the Langmuir model. The Freundlich adsorption isotherm is represented by Eq. 5.

$$\theta = K_{ads} C_{inh}^n \quad (5)$$

Its logarithmic form is Eq.6.

$$\log\theta = \log K_{ads} + n \log C_{inh} \quad (6)$$

where n is an empirical parameter describing the adsorption intensity and surface heterogeneity.

The Temkin adsorption isotherm can be written as Eq. 7.

$$\exp(-2a\theta) = K_{ads} C_{inh} \quad (7)$$

or, in its linear form Eq. 8:

$$\theta = -\frac{1}{2a}\ln K_{ads} - \frac{1}{2a}\ln C_{inh} \quad (8)$$

where a is the molecular-interaction parameter. Its magnitude and sign provide information regarding attractive or repulsive interactions among adsorbed inhibitor species.

The Frumkin adsorption isotherm is given by Eq. 9:

$$\frac{\theta}{1-\theta}\exp(-2a\theta) = K_{ads} C_{inh} \quad (9)$$

The standard Gibbs free energy of adsorption, ΔG^0_{ads}, was calculated from K_{ads} using Eq. 10:

$$\Delta G^\circ_{ads} = -RT\ln(55.5 K_{ads}) \quad (10)$$

where R is the universal gas constant, T is the absolute temperature, and 55.5 represents the molar concentration of water. For this calculation, C_{inh} should be expressed in $Lmol^{-1}$, and K_{ads} should be reported in $Lmol^{-1}$.

2.5. Electrochemical Impedance Spectroscopy (EIS)

Electrochemical impedance spectroscopy measurements were performed using a Gamry REF 600 potentiostat/galvanostat/ZRA controlled by Gamry EIS300 software (Gamry Instruments, Warminster, PA, USA). Impedance data were collected in a jacketed three-electrode cell with mild steel as the working electrode, graphite as the counter electrode, and an SCE reference. After approximately 30 min at open circuit, spectra were recorded at the stabilized potential using a 5 mV peak-to-peak sinusoidal perturbation over a frequency range of 100-0.1 Hz. The resulting impedance spectra were fitted to an appropriate equivalent electrical circuit using Gamry Echem Analyst software. The fitting procedure was used to determine the solution resistance, R_s, charge-transfer resistance, R_{ct}, and constant-phase-element parameters. Each measurement was repeated three times under identical conditions, and the average values were reported. The inhibition efficiency obtained from EIS measurements was calculated using equation 11.

$$IE_{EIS}(\%) = \frac{R_{ct}^{inh} - R_{ct}^0}{R_{ct}^{inh}} \times 100 \quad (11)$$

where R_{ct}^0 and R_{ct}^{inh} are the charge-transfer resistance values measured in the absence and presence of HBAT, respectively.

The corresponding surface coverage was calculated as in equation 12.

$$\theta_{EIS} = \frac{R_{ct}^{inh} - R_{ct}^0}{R_{ct}^{inh}} \quad (12)$$

2.6. Scanning electron microscopy

The surface morphology of mild steel was examined using field-emission scanning electron microscopy. Mild-steel coupons with dimensions of 4.0×2.5×0.1 cm were successively abraded using 400-, 600-, and 1200-grit abrasive papers, rinsed with distilled water, degreased with acetone, and dried before immersion. The specimens were exposed to uninhibited 1 M HCl and to 1 M HCl containing the optimum HBAT concentration of 0.5 mM at 303 K for 5 h. A freshly polished specimen was also examined as a reference surface. Following immersion, the coupons were removed from the solutions, gently rinsed with distilled water, dried, and subjected to surface analysis. The surface images were obtained using a Zeiss MERLIN Compact field-emission scanning electron microscope at the Electron Microscopy Unit, Universiti Kebangsaan Malaysia.

2.7. Computational details

Geometry optimization and electronic-structure calculations for HBAT were performed using GAMESS software and the molecular geometries were optimized usingB3LYP functional along with a 6-31G(d) basis set level. Frontier molecular orbital energies, the energy gap $\Delta E = E_{LUMO}-E_{HOMO}$, electronegativity, global hardness and softness, and the fraction of electrons transferred (ΔN) were calculated using the standard operational Eqs. 13-16.

$$\Delta E = E_{LUMO} - E_{HOMO} \quad (13)$$

$$\eta = \frac{\Delta E}{2} \quad (14)$$

$$\chi = -\frac{E_{HOMO}+E_{LUMO}}{2} \quad (15)$$

$$\Delta N = \frac{\chi_{Fe}-\chi_{PPMT}}{2(\eta_{Fe}+\eta_{PPMT})} \quad (16)$$

where χ_{Fe} and η_{Fe} are the electronegativity and hardness of iron, respectively. A positive ΔN value suggests electron donation from the inhibitor to the metal, enhancing adsorption.

3. Results and Discussions

The following discussion distinguishes two levels of claim. Experimentally demonstrated observations are the gravimetric inhibition efficiencies, the temperature dependence of those efficiencies, the increase in charge-transfer resistance and decrease in effective interfacial capacitance, the Langmuir description of coverage versus concentration, the van't Hoff parameters obtained from $K_{ads}(T)$, and the SEM morphology. Proposed molecular-level explanations mixed physical and chemical adsorption, specific Fe–N, Fe–S, or Fe–O contacts, π–metal interaction, and back-donation are identified as such and are based on HBAT structure, DFT descriptors, and literature precedent. They are not treated as experimentally demonstrated mechanisms.

3.1. Gravimetrical measurements

3.1.1. Effect of concentration and immersion periods

Figure 2 shows the corrosion rate and gravimetric inhibition efficiency of mild steel in 1 M HCl containing HBAT after 1, 5, 10, 24, and 48 h at 303 K. Inhibition efficiency increased with HBAT concentration and with immersion time up to 24 h. This trend is consistent with progressive adsorption, increasing surface coverage, and growth of a compact protective film that restricts access of H^+ and Cl^- to active steel sites. At approximately 0.5 mM the response approached a plateau: increasing the concentration to 1.0 mM produced only a marginal further improvement, indicating that most accessible adsorption sites were already occupied. Beyond 24 h the film remained highly persistent. A slight decrease at 48 h was observed mainly at the lower concentrations, whereas 0.5 mM remained essentially unchanged (96.82 % at 24 h and 96.81 % at 48 h). The small 48 h decrease at low dosage is consistent with limited rearrangement or partial desorption of a weakly bound fraction of the layer, not with collapse of the protective film. Individual numerical values are displayed in Figure 2 and are not restated here [19-23].

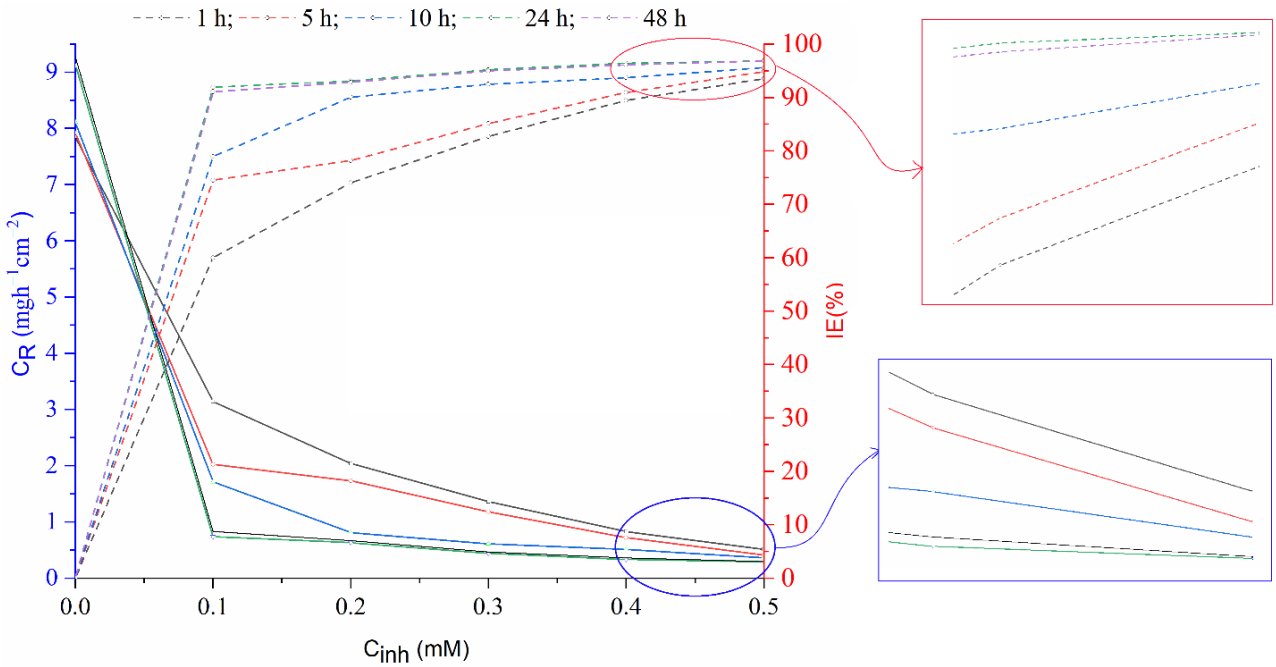


Figure 2: Corrosion rate and gravimetric inhibition efficiency of mild steel in 1 M HCl containing different concentrations of HBAT after 1, 5, 10, 24, and 48 h of immersion at 303 K (mean of three independent measurements).

The increase in inhibition efficiency with temperature was accompanied by a progressive decrease in the corrosion rate of the inhibited specimens. At 0.1 mM HBAT, C_R decreased from 3.14 to 2.11 mgcm^{-2}h^{-1} between 303 and 333 K. At 0.3 mM, it decreased from 1.36 to 0.62 mgcm^{-2}h^{-1} while at 0.5 mM it declined from 0.51 to 0.30 mgcm^{-2}h^{-1}. Thus, although heating accelerated the corrosion of mild steel in the uninhibited acid, it enhanced the relative protective action of HBAT. This behavior indicates that the temperature-assisted adsorption or interfacial bonding of HBAT increased more strongly than the temperature-induced acceleration of steel dissolution. For many physically adsorbed organic inhibitors, increasing temperature promotes desorption from the metal surface and consequently decreases inhibition efficiency. This behavior has been reported for several amino-benzothiazole, oxadiazole, and Schiff-base inhibitors in hydrochloric acid, for which the loss of efficiency at elevated temperature was associated with weakening of the physically adsorbed film and increased exposure of the steel surface to the corrosive medium [20-23]. In contrast, retention or enhancement of inhibition efficiency at elevated temperature has been associated with stronger interactions, inferred from the temperature-dependent inhibition efficiency, between inhibitor molecules and the steel surface. Nataraja et al. similarly suggested that constant or slightly increasing inhibition efficiency at elevated temperature and sufficiently high inhibitor concentration may arise from chemisorption or from the combined contribution of physical and chemical adsorption [19].

Temperature had a clear impact, but it changed with the HBAT amount. From 303 to 333 K, the inhibition efficiency went up much more at 0.1 mM. The small change at the top concentration should not be read as weak response. It fits with the fact that the efficiency was already high at 303 K, about 93.50%. So there was little room to improve further. With 0.5 mM, many corrosion sites were likely taken even at the lower temperature. That leaves fewer empty spots for extra adsorption. Because of this, the inhibition level moved toward a flat region near 97%. This points to almost full coverage of the electrochemically active surface. At the low HBAT levels, heating seems to help. It likely made it easier for HBAT molecules to reach the surface and adsorb onto sites that were still open. Heat may also help the molecules line up in a better way. Figure 3 shows the effect of temperature (303-333 K) on the corrosion rate and inhibition efficiency of mild steel in 1 M HCl containing 0.1-0.5 mM HBAT after 5 h. The blank corrosion rate increased with temperature, as expected for thermally accelerated acid attack. In the presence of HBAT,

inhibition efficiency increased with both concentration and temperature, reaching 96.65 % at 0.5 mM and 333 K, while the inhibited corrosion rate decreased. This behaviour differs from that of many predominantly physically adsorbed inhibitors, whose protection commonly falls on heating. The present trend is consistent with temperature-assisted adsorption and with a growing contribution of donor–acceptor interactions, but it does not by itself prove chemical bonding. Direct FTIR or XPS evidence of Fe–N, Fe–S, or Fe–O bonds is not available. The thermodynamic nature of the adsorption process is therefore assessed from the temperature dependence of K_{ads} using the van't Hoff relation, as described in the following subsection. Individual numerical values are shown in Figure 3.

3.1.2. Adsorption thermodynamics and van't Hoff analysis

The temperature dependence of HBAT adsorption on mild steel in 1 M HCl was evaluated from the gravimetric data at 303, 313, 323 and 333 K. Surface coverage at each temperature was obtained from the corresponding inhibition efficiency, and the adsorption equilibrium constant, K_{ads}, was determined from the intercept of the linear Langmuir plot of C/θ versus C. The standard Gibbs free energy of adsorption was then calculated from using equation 10.

The resulting parameters are collected in Table 1. K_{ads} increased from 1.27×10^4 M^{-1} at 303 K to 2.98×10^4 M^{-1} at 333 K, while $\Delta G°_{ads}$ became steadily more negative (-33.93 to -39.64 kJ mol^{-1}). Adsorption of HBAT is therefore spontaneous over the investigated window, and heating favors the adsorbed state. The magnitude of $\Delta G°_{ads}$ lies between the ranges commonly associated with exclusive physisorption and exclusive chemisorption, and is therefore consistent with mixed-mode adsorption involving both electrostatic interaction and donor–acceptor contributions. In the absence of FTIR or XPS of the adsorbed film, this thermodynamic classification remains an inference and does not identify specific Fe–N, Fe–S or Fe–O bonds. The standard enthalpy and entropy of adsorption were obtained from a single van 't Hoff regression of ln K_{ads} against $1/T$, (Eq. 17)

$$\ln K_{ads} = \Delta S°_{ads}/R - \Delta H°_{ads}/\mathrm{RT} \qquad (17)$$

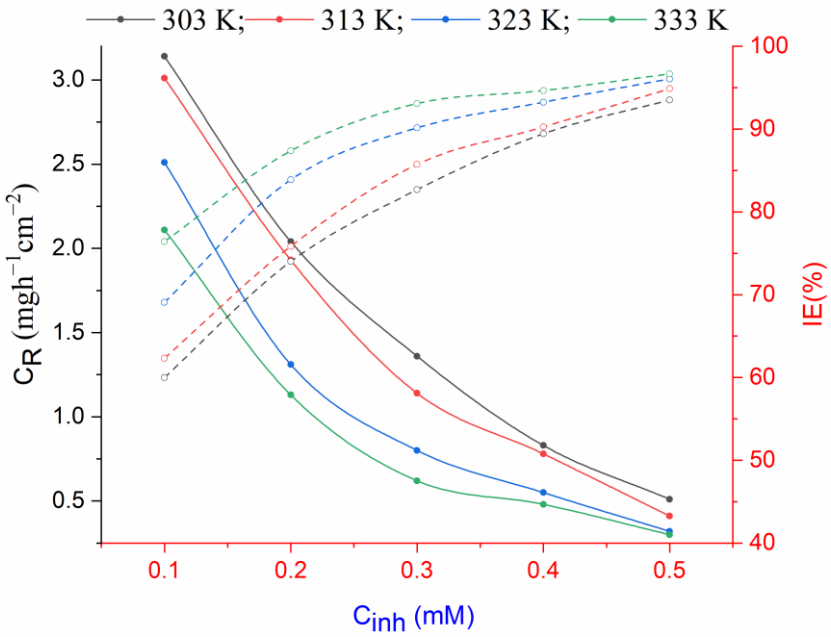


Figure 3: Effect of temperature and HBAT concentration on the corrosion rate and gravimetric inhibition efficiency of mild steel in 1 M HCl (mean of three independent measurements).

The plot is linear (Figure 4; $R^2 = 0.9982$). Because ΔH^0_{ads} and ΔS^0_{ads} are defined by one slope and one intercept, they are reported once for the 303-333 K interval and are not restated as independent values at each temperature (Table 1). The fit yields ΔH^0_{ads}= +23.73 kJ mol^{-1} and ΔS^0_{ads} = +190.2 J mol^{-1} K^{-1}. The positive enthalpy shows that adsorption of HBAT is endothermic under the present conditions, in agreement with the experimental rise in both K_{ads} and inhibition efficiency on heating (93.50 % at 303 K to 96.65% at 333 K for 0.5 mM HBAT). The large positive entropy is consistent with an increase in interfacial disorder as water molecules are displaced from the steel surface when HBAT adsorbs. Taken together, the van't Hoff analysis shows that adsorption of HBAT is spontaneous and endothermic under the investigated conditions. The magnitude of $\Delta G°_{ads}$ is consistent with a mixed electrostatic and donor–acceptor contribution. This thermodynamic classification is an inference from $K_{ads}(T)$ and does not identify specific Fe–N, Fe–S, or Fe–O bonds.

Table 1: Langmuir adsorption equilibrium constants and standard free energies of adsorption for HBAT on mild steel in 1 M HCl, together with the van 't Hoff enthalpy and entropy obtained from a single linear fit.

T (K)	K_{ads} (M^{-1})	R^2 (Langmuir)	$\Delta G°_{ads}$ (kJ mol^{-1})
303	1.27×10^4	0.9987	−33.93
313	1.68×10^4	0.9996	−35.77
323	2.22×10^4	0.9998	−37.65
333	2.98×10^4	0.9998	−39.64

van 't Hoff parameters (one pair for 303–333 K, Figure 4): $\Delta H°_{ads}$ = +23.73 kJ mol^{-1}; $\Delta S°_{ads}$ = +190.2 J mol^{-1} K^{-1}; R^2 = 0.9982.

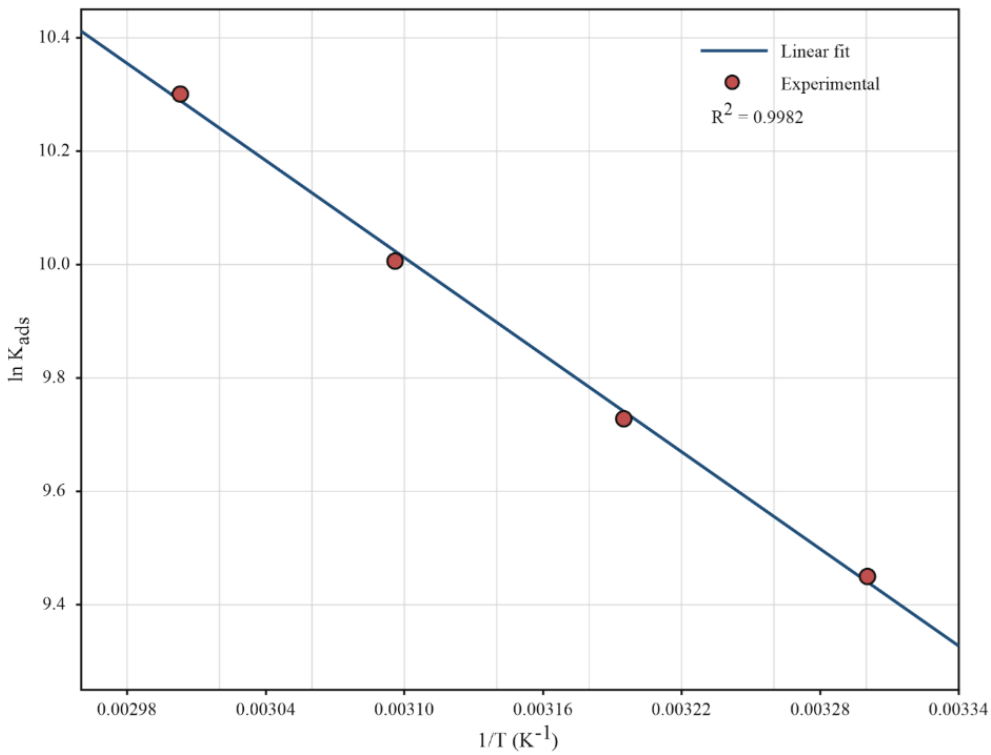


Figure 4: van 't Hoff plot of ln K_{ads} versus 1/T for HBAT adsorption on mild steel in 1 M HCl at 303-333 K. Symbols are experimental Langmuir constants; the solid line is the linear fit (R^2 = 0.9982).

3.1.3. Adsorption isotherm

The corrosion-inhibition action of HBAT is principally associated with its adsorption at the mild-steel/solution interface and the consequent displacement of water molecules and aggressive species from electro-chemically active sites. The fractional surface coverage, θ, was calculated from the gravimetric results obtained after 5 h of immersion at 303 K according to Equation 3. The blank solution was excluded from the adsorption-isotherm fitting because both the inhibitor concentration and surface coverage are zero [27]. The calculated surface-coverage values and the corresponding Lang-muir parameters are presented in Figure 5.

At 5 h, the estimated coverage rose from 0.7449 at 0.1 mM to 0.9482 at 0.5 mM, consistent with increasingly complete occupation of reactive regions as more inhibitor became available. Consequently, the effective area exposed to H^+, Cl^-, and water molecules decreased, accounting for the simultaneous reduction in corrosion rate and improvement in inhibition efficiency. To establish the adsorption behavior of HBAT, the experimental surface-coverage data were fitted to the Langmuir, Freundlich, Temkin, and Frumkin models using equations 4-9. The statistical parameters obtained from the linearized forms are compared in Table 2.

Of the four linearized isotherms, Langmuir gave the strongest fit (R^2 = 0.9948) and a slope of 0.9702. It is therefore the most useful macroscopic description of the data and is consistent with near-monolayer coverage, although it does not prove that every surface site is identical and that each adsorbed molecule occupies a defined fraction of the available surface. The model further assumes comparable adsorption energies at the occupied sites and negligible interactions between neighboring adsorbed species. High R^2 values and slopes close to unity have similarly been interpreted as evidence of Langmuir-type adsorption on steel surfaces. Nevertheless, the mild-steel surface is not perfectly homogeneous, and the slope differs slightly from one [28]. Therefore, the Langmuir model should be regarded as the best macroscopic approximation to the experi-mental data rather than proof of an entirely ideal and homogeneous surface.

The adsorption equilibrium constant was obtained from the intercept of the Langmuir plot (Eq. 18).

$$\text{intercept} = \frac{1}{K_{\text{ads}}} \qquad (18)$$

Because Figure 5 was plotted using concentration in mM, the intercept of 0.05092 mM was first converted to 5.092×10^{-5} $molL^{-1}$. The calculated adsorption equilibrium constant was therefore (Eq. 19).

$$K_{\text{ads}} = \frac{1}{5.092\times10^{-5}} = 1.964 \times 10^4 \text{ L mol}^{-1} \qquad (19)$$

The relatively high K_{ads} value indicates a strong adsorption affinity of HBAT toward the mild-steel surface and the formation of a stable adsorbed layer. In adsorption-isotherm analysis, a larger equilibrium constant corresponds to stronger adsorption of inhibitor molecules at the metal/solution interface.

The standard Gibbs free energy of adsorption was calculated using Eq. 20, the substitution of K_{ads}= 1.964×10^4 $molL^{-1}$ at 303 K.

$$\Delta G^{\circ}_{\text{ads}} = -35.02 \text{ kJ mol}^{-1} \qquad (20)$$

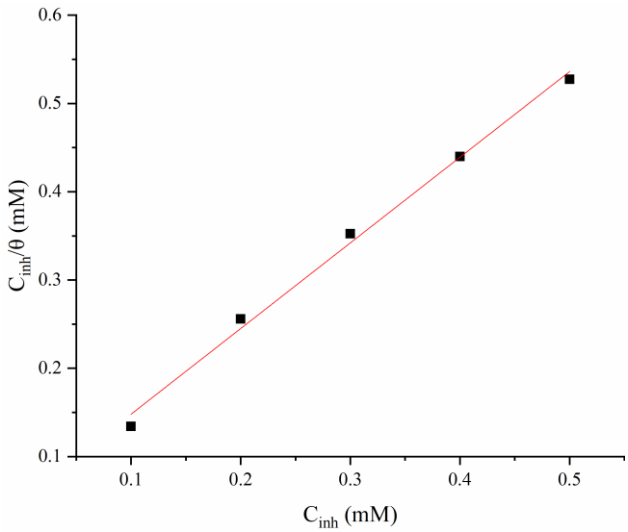


Figure 5: Langmuir adsorption isotherm obtained by plotting C_{inh}/θ against C_{inh} for HBAT adsorption on mild steel in 1 M HCl after 5 h of immersion at 303 K.

Table 2: Comparison of the adsorption-isotherm models applied to HBAT adsorption on mild steel in 1 M HCl at 303 K.

Adsorption model	Principal fitted parameter	Parameter value	(R^2)
Langmuir	Slope	0.9702	0.9948
Freundlich	(n)	0.1540	0.9430
Temkin	(a)	-3.879	0.9313
Frumkin	(a)	0.755	0.1854

The negative adsorption free energy shows that transfer of HBAT from solution to the steel surface is spontaneous. Its intermediate magnitude is more consistent with combined electrostatic and donor-acceptor contributions than with an exclusively physical or exclusively chemical pathway. A comparable interpretation was reported in the attached furan-derivative study, in which an intermediate adsorption free energy was attributed to contributions from both physisorption and chemisorption. Chloride adsorption can create interfacial regions that attract protonated HBAT, providing an electrostatic adsorption route. Neutral HBAT may additionally bind to iron through its N, S, and O donor sites and delocalized π electrons. Together, these interactions can produce a compact film that blocks both anodic and cathodic reaction sites. These simultaneous interactions would account for the high K_{ads}, the negative ΔG^0_{ads}, and the strong inhibition efficiency observed gravimetrically. The Freundlich model gave a lower coefficient of determination, R^2=0.9430, indicating that adsorption on an energetically heterogeneous surface does not describe the experimental data as accurately as the Langmuir model. The Temkin plot had weaker straight-line behavior. The fit gave R^2=0.9313, This points to the idea that changes in adsorption energy from side by side adsorbates are not the main effect in the HBAT system. The Frumkin model did not match well at all. Its R^2=0.1854, was only 0.1854. Because of that, it could not reflect the adsorption trend across the tested concentration window. Langmuir was used for another reason too. It was not picked just because the regression looked best. Its slope was near 1, and the fitted values matched what we saw as the surface coverage rose step by step. Model selection should consider both statistical agreement and the physical reasonableness of the resulting parameters rather than comparing K_{ads} values alone, since equilibrium constants obtained from different model formulations are not always directly comparable [27-29]. The attached literature likewise emphasizes that both regression quality and physicochemical consistency should be considered when identifying the most representative adsorption model. Overall, the Langmuir model provides the most useful macroscopic description of the concentration dependence of surface coverage. The high K_{ads} and negative $\Delta G°_{ads}$ support spontaneous adsorption of HBAT and are consistent with formation of an approximately monolayer film. These results support the occurrence and affinity of adsorption. They do not establish a particular chemical adsorption mechanism or specific metal-inhibitor bonds.

3.2. EIS

Electrochemical impedance spectroscopy was employed to evaluate the interfacial behavior of mild steel in 1 M HCl in the absence and presence of different HBAT concentrations. The equivalent electrical circuit used to fit the impedance spectra is shown in Figure 6a, whereas the corresponding Nyquist plots are presented in Figure 6b.

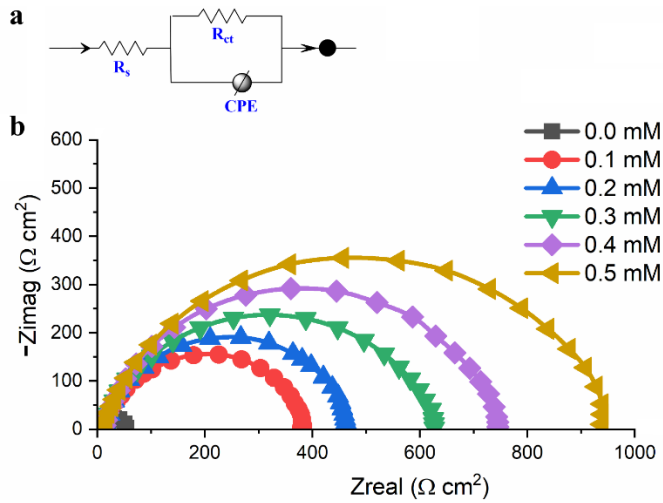


Figure 6: (a) Equivalent electrical circuit used to fit the EIS data and (b) Nyquist plots for mild steel in 1 M HCl in the absence and presence of different concentrations of HBAT at 303 K.

The circuit consists of the solution resistance, R_s, connected in series with a parallel combination of the charge-transfer resistance, Rct_s, and a constant-phase element, CPE: R_s-R_{ctlCPE} This circuit is commonly used to describe corrosion systems controlled predominantly by charge transfer at the metal/solution interface. A constant-phase element was used because roughness, adsorption, and surface heterogeneity produce a non-ideal capacitive response. Every spectrum retained one depressed semicircle; thus, HBAT reduced the rate of the existing charge-transfer process without changing its basic form. Instead, HBAT suppresses the rate of the existing charge-transfer process by adsorbing on the metal surface. The depressed character of the semicircles, rather than perfectly ideal semicircular behavior, is attributed to the heterogeneous nature of the mild-steel surface and to the distribution of relaxation times at the steel/ electrolyte interface. Similar depressed capacitive loops have been reported for inhibited mild-steel systems and are commonly represented using a CPE-containing equivalent circuit [22, 31]. The diameters of the capacitive loops increased markedly with increasing HBAT concentration. The smallest loop was observed for mild steel immersed in the uninhibited acid, while the largest semicircle was obtained at 0.5 mM HBAT. Because the diameter of the capacitive loop is directly related to the charge-transfer resistance, this progressive enlargement indicates increasing resistance to electron transfer and iron dissolution at the steel/solution interface [32, 33]. The EIS parameters obtained from equivalent-circuit analysis are summarized in Table 3.

The R_s values ranged from 1.02 to 2.72 Ωcm^2, with no systematic dependence on HBAT concentration. These relatively small variations indicate that the addition of HBAT had only a limited influence on the bulk resistance of the acidic solution. Variations in R_s may also arise from small differences in the relative positions of the working and reference electrodes or from experimental fluctuations in solution conductivity. Consequently, the principal changes in the impedance response are associated with the metal/solution interface rather than the resistance of the electrolyte [33]. A pronounced concentration-dependent increase in R_{ct} was observed. The charge-transfer resistance increased from 47.53 Ωcm^2 for the uninhibited solution to 381.58 Ωcm^2 at only 0.1 mM HBAT. Further increases in concentration produced R_{ct} values of 462.25, 633.73, 752.11, and 933.25 Ωcm^2 at 0.2, 0.3, 0.4, and 0.5 mM, respectively. Thus, the value obtained at 0.5 mM was approximately 19.6 times greater than that of the blank solution.

With HBAT on the surface, there are fewer free spots for anodic iron to dissolve. There are also fewer spots for cathodic hydrogen to form. When the HBAT level goes up, more of the surface gets covered. This makes the protective layer more even and harder for the corrosion process to pass through. This same trend matches earlier EIS reports. In those works, higher inhibitor dose gave bigger capacitive loops and larger charge transfer resistance [34]. The reason was adsorption and loss of active sites. Inhibition efficiency was worked out from the charge transfer resistance using equation 11. As listed in Table 3, the efficiency went from 87.54% at 0.1 mM to 94.91% at 0.5 mM. So the top value matches the largest R_{ct} and the biggest Nyquist arc seen in Figure 6b. Overall, the data show that corrosion control improves step by step as more adsorbed HBAT remains on the surface. For the blank solution, the CPE exponent n was 0.57.

Table 3: Electrochemical impedance parameters for mild steel in 1 M HCl in the absence and presence of different HBAT concentrations at 303 K.

HBAT (mM)	R_S (Ωcm^2)	R_{ct} (Ωcm^2)	$CPE_{dl}\ Y_0$ ($\Omega^{-1}\ s^n cm^{-2}$)	(n)	C_{dl}($\mu F cm^{-2}$)	IE (%)
0.0 mM	1.02	47.53	925.6	0.57	925.6	0.00
0.1 mM	1.51	381.58	611.6	0.79	611.6	87.54
0.2 mM	2.14	462.25	458.4	0.74	458.4	89.72
0.3 mM	1.90	633.73	565.9	0.77	565.9	92.50
0.4 mM	2.72	752.11	523.2	0.84	523.2	93.68
0.5 mM	1.95	933.25	413.4	0.75	413.4	94.91

That points to strong non-ideal capacitive behavior. One reason is the rough, highly mixed steel surface after exposure to uninhibited 1 M HCl. When HBAT was added, n moved higher to about 0.74 to 0.84. This general increase suggests the steel solution boundary becomes more even. It also brings the response closer to ideal capacitive behavior. The best case was at 0.4 mM, where, n reached, 0.84. This suggests that this dose formed a relatively uniform film on the interface [35]. Small changes in the inhibitor level are not proof of how well the inhibition works. The CPE exponent can shift for other reasons too. For example, surface roughness matters. So does porosity. How adsorption is spread across the area can change the result. Local differences in the dielectric constant also play a role. The protective film may not be uniform, and that can affect the outcome as well. Thus, the decrease from 0.84 at 0.4 mM to 0.75 at 0.5 mM may reflect differences in the organization or local distribution of the adsorbed HBAT layer rather than deterioration of its protective performance. The simultaneous increase in $R_{ct}$and inhibition efficiency at 0.5 mM confirms that this concentration still provides the strongest overall corrosion resistance [36]. The effective double-layer capacitance decreased substantially after addition of HBAT. The value declined from 925.6 μFcm^{-2} for the blank to 611.6 μFcm^{-2} at 0.1 mM and reached 413.4 μFcm^{-2} at 0.5 mM. The overall decrease in C_{dl} may be interpreted using the Helmholtz relationship (Eq. 21) [30].

$$C_{dl} = \frac{\varepsilon\varepsilon_0 A}{d} \quad (21)$$

where ε is the local dielectric constant, ε_0 is the vacuum permittivity, $A$is the effective interfacial area, and d is the thickness of the electrical double layer. A reduction in C_{dl} may therefore result from a decrease in the local dielectric constant as adsorbed water molecules are replaced by organic HBAT molecules, an increase in the thickness of the protective interfacial layer, or both. The decrease in double-layer capacitance following inhibitor adsorption has similarly been attributed to the formation of a thicker protective film and changes in the dielectric properties of the interface. The C_{dl} values did not decrease perfectly monotonically at all intermediate concentrations. For instance, C_{dl} increased from 458.5 μFcm^{-2} at 0.2 mM to 565.9 μFcm^{-2} at 0.3 mM before decreasing again at higher concentrations. The changes you observe may be due to the stability of the inhibitor, the cohesion of the surrounding layer, and the degree of surface unevenness. These changes may also reflect a problem in converting the imperfect capacitance curve into a usable capacitance value. Therefore, the overall trend of the capacitance results should be considered, rather than expecting a gradual and constant increase or decrease. The values drop overall, from 925.6 down to 413.4 μFcm^{-2}, At the same time, R_{ct}, rises clearly. This points to an adsorbed HBAT film that helps protect the steel surface. The EIS data match what the mass measurements show. In both tests, the protection improves as the HBAT level goes up, and it peaks at 0.5 mM. Several EIS signs line up together. The charge transfer resistance goes higher. The double layer capacitance goes down. The Nyquist arc gets larger. Taken as a whole, these results suggest that HBAT sticks well to the mild-steel surface in the solution. It also acts as a blocking layer that limits corrosion caused by the acid. EIS was performed at 303 K. Temperature-dependent impedance spectra were not recorded; the temperature response of HBAT adsorption is therefore discussed from the gravimetric K_{ads}(T) data using the van't Hoff relation. The calculated and experimental Nyquist overlays were inspected for each spectrum, and the fit was accepted when the overlay reproduced the experimental loop. Numerical goodness-of-fit (χ2) values are not reported.

3.3. DFT analysis and relationship with corrosion inhibition

Density functional theory calculations were employed to provide molecular-level insight into the corrosion-inhibition behavior of HBAT toward mild steel in 1 M HCl. The optimized molecular geometry and frontier molecular orbitals obtained at the B3LYP/6-31G(d) level are presented in Figure 7. Frontier molecular orbital analysis is widely used to rationalize corrosion-inhibitor adsorption because the highest occupied molecular orbital (HOMO) is associated with the ability of a molecule to donate electron density, whereas the lowest unoccupied molecular orbital (LUMO) reflects its ability to accept electron density from the metal surface. These donor–acceptor interactions can contribute to adsorption and stabilization of an organic inhibitor at the steel/solution interface. For HBAT, the calculated HOMO and LUMO energies were -8.355 and -1.743 eV, respectively, giving a HOMO–LUMO energy separation of Eq. 22.

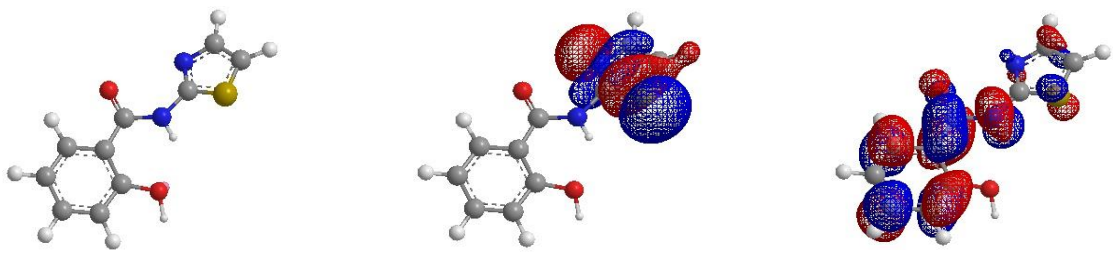
$\Delta E = E_{LUMO} - E_{HOMO} = (-1.743) - (-8.355) = 6.612$ eV (22)

In general, a higher E_{HOMO} facilitates electron donation to vacant Fe orbitals, whereas a lower E_{LUMO} favors acceptance of electron density from occupied metal orbitals. Likewise, lower HOMO–LUMO gaps are commonly associated with greater molecular softness and easier redistribution of electron density during adsorption. However, the relatively large gap obtained for HBAT (6.612 eV) should not, by itself, be described as evidence of unusually high chemical reactivity. Because only one inhibitor molecule is being considered here, ΔE is better interpreted together with the spatial distribution of the frontier orbitals, heteroatom donor sites, adsorption measurements, and electrochemical results rather than as an independent predictor of inhibition efficiency. The frontier-orbital distributions provide particularly useful information about the possible HBAT–Fe interaction. As shown in Figure 7, the HOMO electron density is concentrated predominantly around the N- and S-containing heterocyclic portion of HBAT and the adjacent conjugated region. This distribution identifies these sites as probable electron-donating centers. The lone-pair electrons associated with the heteroatoms, together with the π-electron density of the conjugated system, can interact with vacant Fe 3*d* states during adsorption. In contrast, the LUMO is more extensively distributed over the aromatic/conjugated framework, including the carbonyl-containing region and heterocyclic moiety. Such a distribution indicates that HBAT can also accommodate electron density transferred from occupied Fe orbitals. Similar donor-acceptor interactions involving N, O and S atoms and aromatic π systems have been widely invoked in the adsorption of organic corrosion inhibitors on steel surfaces.

The global reactivity descriptors calculated from the frontier orbital energies further characterize the electronic properties of HBAT. Table 4 shows the calculated frontier molecular orbital energies and global quantum-chemical reactivity descriptors of HBAT at the B3LYP/6-31G(d) level.

Table 4: Calculated frontier molecular orbital energies and global quantum-chemical reactivity descriptors of HBAT at the B3LYP/6-31G(d) level.

Quantum descriptor	HBAT value
E_{HOMO} (eV)	−8.355
E_{LUMO} (eV)	−1.743
ΔE (eV)	6.612
Ionization potential, I (eV)	8.355
Electron affinity, A (eV)	1.743
Electronegativity, χ (eV)	5.049
Global hardness, η (eV)	3.306
Global softness, σ (eV^{-1})	0.302
ΔN, using χ_{Fe}= 7.0 eV and η_{Fe}=0	+0.295



Optimized Structure **HOMO** **LUMO**

Figure 7: Optimized molecular structure and frontier molecular orbital distributions (HOMO and LUMO) of HBAT calculated at the B3LYP/6-31G(d) level.

The calculated global hardness of 3.306 eV and softness of 0.302 eV^{-1} indicate that the electronic density of HBAT can undergo redistribution upon interaction with the metal surface, although the relatively large HOMO–LUMO gap shows that the isolated neutral molecule also possesses appreciable electronic stability. Therefore, the corrosion-inhibiting ability of HBAT is more reasonably attributed to the combination of its heteroatom-rich adsorption centers, conjugated π system, and ability to participate in reciprocal charge-transfer interactions rather than to exceptionally high intrinsic softness alone. Using the bulk-iron approximation frequently employed in corrosion-inhibitor studies, χ_{Fe}=7.0 eV and η_{Fe}=0, the fraction of transferred electrons is calculated as (Eq. 23).

$$\Delta N=\frac{\chi_{Fe}-\chi_{HBAT}}{2(\eta_{Fe}+\eta_{HBAT})}=\frac{7.0-5.049}{2(3.306)}=0.295 \quad (23)$$

The positive value of ΔN under this convention indicates a predicted tendency for electron-density transfer from HBAT toward iron, supporting coordination of the inhibitor with the metal through its donor atoms and π system. Positive ΔN values are frequently interpreted in corrosion-inhibitor studies as evidence of donor interaction with the metallic surface. It should nevertheless be emphasized that $\Delta N$is a conceptual DFT descriptor rather than the literal number of electrons experimentally transferred between an isolated molecule and the steel surface. The combined HOMO and LUMO distributions suggest a synergistic adsorption mechanism. Electron donation from the N, S, O and conjugated π centers of HBAT toward available Fe orbitals can strengthen inhibitor adsorption, while the accessible LUMO may permit reciprocal Fe-to-inhibitor back-donation. The resulting donor–acceptor interactions can stabilize the adsorbed HBAT layer and increase surface coverage, thereby limiting the access of aggressive H^+ and Cl^- species to electrochemically active sites on mild steel. This interpretation provides a molecular rationale for the protective behavior determined experimentally by weight-loss, EIS, adsorption, and surface-characterization measurements. In particular, formation of an adsorbed organic layer would be expected to suppress metal dissolution and charge-transfer processes, consistent with the enhanced corrosion resistance observed experimentally for HBAT. The acidic environment should also be considered when interpreting the calculations. In 1 M HCl, protonation of one or more heteroatomic sites of HBAT is plausible, while chloride ions may participate in the interfacial adsorption process. Consequently, adsorption may contain both chemical and electrostatic contributions: neutral HBAT molecules can interact directly with Fe through heteroatom lone pairs and π electrons, whereas protonated HBAT species may be stabilized near chloride-covered regions of the interface. Calculations on corrosion inhibitors have shown that protonation can substantially alter HOMO/LUMO energies, hardness, softness, dipole moment, and the preferred charge-transfer mechanism. The present B3LYP/6-31G(d) calculation is therefore consistent with a proposed donor–acceptor adsorption mode involving the N, S, and O centres and the aromatic π-system. It does not experimentally identify surface bonds and is not a stand-alone quantitative prediction of inhibition efficiency.

3.4. Surface analysis

Figure 8 shows how the surface looks after 5 h of soaking in 1 M HCl at 303 K. The figure compares the mild steel without HBAT and with 0.5 mM HBAT. The two images look very different, which fits the idea that HBAT has a protective role at the mild-steel and acid boundary. In Figure 8A, the sample treated with uninhibited 1 M HCl has a badly damaged surface. It looks rough and uneven across the whole area shown. There are many signs of wear, including cracks, pits, cavities, and uneven deposits. Corrosion products also gather in clusters. There are also clear local holes and breaks in the surface. These features suggest strong acid attack. They also show that the mild steel did not dissolve in a uniform way. The observed shape changes are linked to steady anodic iron loss. At the same time, weakly attached corrosion products build up during contact with hydrochloric acid. Some SEM results for mild steel in HCl have been described before. In that work, the metal was not inhibited, and the acid attack led to heavy cracking, pitting, and clear harm to the surface [37]. Here, the sample kept in 1 M HCl with 0.5 mM HBAT looks different. Its surface looks smoother and more even, like the image in Figure 8B shows. The uninhibited piece had strong deposits, cracks, and clear holes. Those features do not show up much on the HBAT-treated surface. Also, the old scratch lines from polishing can still be seen across a lot of the sample. That means the steel was not dissolving as much as before. Only a limited number of small surface

irregularities and isolated particles are visible, demonstrating that HBAT markedly reduced both general and localized corrosion damage [38]. The improved morphology of the inhibited specimen is consistent with the adsorption of HBAT molecules and the development of a compact protective layer over the mild-steel surface. This adsorbed layer restricts direct contact between the steel substrate and corrosive species such as H^+ and Cl^-, thereby reducing the number of active sites available for anodic iron dissolution and cathodic hydrogen evolution. Similar changes from a severely damaged uninhibited surface to a smoother inhibited surface with fewer cracks and pits have been attributed to the formation of an adsorbed corrosion-inhibitor film.

These adsorption centers may interact with the mild-steel surface through electrostatic attraction and donor–acceptor interactions, promoting the formation of a persistent interfacial film. Related heteroatom-containing inhibitors have been described as adsorbing through physical interactions and electron donation to vacant orbitals of surface iron atoms, thereby shielding the metal from corrosive ions [37, 38]. The SEM observations are consistent with the gravimetric and electrochemical results and indicate reduced surface damage, not a specific chemical bond. At 0.5 mM HBAT, the substantial increase in R_{ct} from 47.53 to 933.25 Ωcm^2, together with the decrease in Cdl from 925.6 to 413.4 μFcm^{-2}, indicates the development of a thicker and more resistive interfacial barrier. The corresponding EIS inhibition efficiency of 94.91% is consistent with the marked reduction in surface damage observed in Figure 8B. The gravimetric inhibition efficiency of 94.82 % after 5 h further supports the morphological evidence.

3.5. Suggested mechanism

The corrosion-inhibition behavior of HBAT can be explained by its adsorption at the mild-steel/1 M HCl interface and the subsequent formation of a protective molecular film, as schematically illustrated in Figure 9. The proposed mechanism involves the combined contributions of physical and chemical adsorption. This interpretation is consistent with the Langmuir behaviour, $\Delta G°_{ads}$, the temperature-dependent gravimetric results, the increase in R_{ct}, the decrease in C_{dl}, and the smoother SEM morphology; these data confirm adsorption and film formation, not specific Fe–heteroatom bonds. In uninhibited 1 M HCl, corrosion proceeds through anodic dissolution of iron and cathodic hydrogen evolution as in equations 24 and 25.

$$Fe \rightarrow Fe^{2+} + 2e^- \quad (24)$$

$$2H^+ + 2e^- \rightarrow H_2 \quad (25)$$

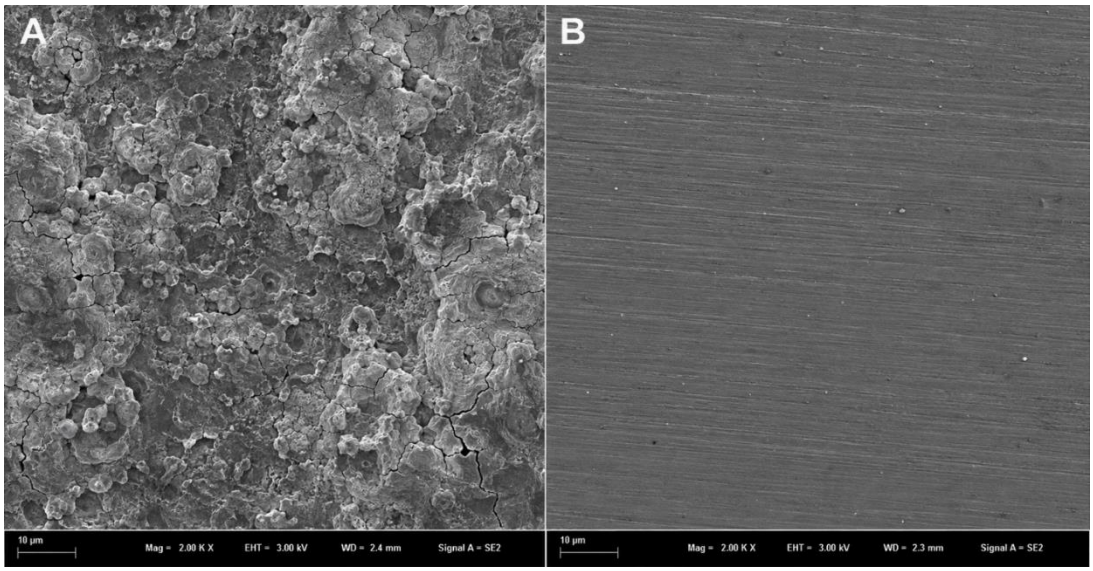


Figure 8: SEM micrographs of mild-steel surfaces after immersion for 5 h at 303 K in: (A) uninhibited 1 M HCl and (B) 1 M HCl containing 0.5 mM HBAT. The images are morphological evidence of reduced acid attack; they do not identify the chemical composition of the surface layer.

Chloride ions promote steel dissolution by adsorbing at the metal/solution interface and participating in the formation of soluble iron-chloride species. In the absence of HBAT, the continuous access of H^+ and Cl^- to the surface sustains the anodic and cathodic reactions, leading to the extensive surface deterioration observed in the uninhibited SEM micrograph. HBAT contains several electron-rich adsorption centers, including the phenolic oxygen, carbonyl oxygen, amide nitrogen, thiazole nitrogen, thiazole sulfur, and the delocalized π-electron systems of the aromatic and heterocyclic rings. Electron-donating heteroatoms and aromatic π-systems are recognized as important adsorption centers in thiazole-based corrosion inhibitors because they facilitate interaction with metal surfaces and promote protective-film formation. The structure of HBAT therefore enables adsorption through more than one interaction pathway [37-40]. In strongly acidic solution, HBAT may coexist in neutral and protonated forms. Protonation is expected primarily at the more basic heteroatomic centers of the molecule, although the relative population of the different protonated species cannot be established without speciation calculations. At the same time, chloride ions can adsorb on positively charged regions of the mild-steel surface, producing a locally negative interfacial layer. Electrostatic attraction can then develop between protonated HBAT species and the chloride-covered steel surface as in equation 26.

$$Fe\text{-}Cl^-_{ads} + HBATH^+ \rightleftharpoons Fe\text{-}Cl^-_{ads} \cdots HBATH^+ \quad (26)$$

This interaction represents the physisorption pathway shown on the left-hand side of Figure 9. A comparable mechanism has been proposed for aminothiazole inhibitors in 1 M HCl, where chloride adsorption produces a negatively charged interfacial layer that facilitates electrostatic attraction of protonated inhibitor species [39, 40]. The resulting physically adsorbed species can block cathodic sites and restrict the access of hydrogen ions to the steel surface. Consequently, the reduction of H^+ and the evolution of hydrogen gas are suppressed. Related aminothiazole studies similarly indicate that adsorption of protonated species at cathodic sites reduces the availability of these sites for hydrogen-ion reduction. Neutral HBAT molecules may also interact directly with surface iron atoms through donor–acceptor bonding. The lone electron pairs located on the phenolic and carbonyl oxygen atoms, the thiazole nitrogen and sulfur atoms, and, to a lesser extent, the amide functionality can donate electron density to vacant or partially vacant Fe 3dorbitals (equation 27):

$$HBAT{:}+Fe \rightarrow HBAT \rightarrow Fe \quad (27)$$

The conjugated aromatic and thiazole π-electron systems may also contribute to adsorption by interacting with the iron surface. Related studies of aminothiazoles attribute chemisorption to coordination between vacant Fe d-orbitals and the lone electron pairs of nitrogen and sulfur atoms, together with interactions involving aromatic π-electrons. Computational results for a benzothiazole derivative further showed preferential interaction through sulfur and nitrogen and a flattened molecular orientation that maximizes contact with the Fe surface. A synergistic back-donation interaction may additionally occur, in which electron density from occupied Fe d-orbitals is transferred toward suitable antibonding or π* orbitals of HBAT (equation 28):

$$Fe(d) \rightarrow HBAT(\pi^*) \quad (28)$$

Such donation and back-donation interactions can strengthen adsorption and favor a nearly parallel orientation of HBAT relative to the steel surface, allowing several adsorption centers to interact simultaneously. Because FTIR and XPS of the adsorbed layer were not performed, the individual Fe–O, Fe–N, and Fe–S contacts should be regarded as a plausible adsorption mode rather than as spectroscopically identified bonds. DFT descriptors reported in this work are consistent with electron donation from the N, S, and O centres and the aromatic π-system, but they do not replace surface spectroscopy [39, 40]. The relatively high adsorption equilibrium constant and the negative standard Gibbs free energy, ΔG°_{ads}=-35.02 KJmol^{-1} indicate spontaneous and strong adsorption. The intermediate magnitude of ΔG°_{ads}, between values generally associated with purely physical and purely chemical adsorption, supports a mixed adsorption mechanism. A similar interpretation has been reported for aminothiazole adsorption when thermodynamic and molecular simulations indicated contributions from both physisorption and chemisorption. The good agreement with the Langmuir isotherm suggests that the protective action is dominated by the formation of an approximately monomolecular adsorbed layer. As the HBAT concentration increases, more active sites become

occupied, decreasing the exposed metallic area and restricting the transport of H^+, Cl^-, and dissolved iron species across the interface. The progressive increase in inhibition efficiency with immersion time indicates that this film continues to organize and stabilize during exposure. The proposed mechanism is also consistent with the EIS results. Increasing the HBAT concentration from 0 to 0.5 mM increased R_{ct} from 47.53 to 933.25 Ωcm^2, while Cdl decreased from 925.6 to 413.4 μFCm^{-2}. The increase in R_{ct} demonstrates that the adsorbed film strongly impedes interfacial charge transfer, whereas the reduction in Cdl is consistent with displacement of interfacial water molecules, a decrease in the local dielectric constant, and an increase in the effective thickness of the electrical double layer. Studies of related inhibitors similarly associate formation of a stable adsorbed layer with delayed charge transfer and increased interfacial resistance. The SEM observations provide additional support for the barrier mechanism. The severely damaged, cracked, and deposit-covered surface produced in uninhibited HCl was replaced by a substantially smoother and less deteriorated morphology in the presence of 0.5 mM HBAT. This preservation of the surface indicates that the adsorbed inhibitor layer reduces direct contact between the steel substrate and the acidic environment.

The improved inhibition efficiency at elevated temperature is consistent with temperature-assisted, endothermic adsorption. It may include a growing contribution of donor-acceptor interactions, but this is a possible interpretation rather than a demonstrated strengthening of chemical bonds. This behavior is consistent with a mixed adsorption hypothesis involving an initial physical contribution and a possible chemically adsorbed contribution. Overall, HBAT is proposed to inhibit mild-steel corrosion by forming an adsorbed interfacial film through complementary physical and chemical interactions. Overall, HBAT is proposed to inhibit mild-steel corrosion by forming an adsorbed interfacial film. Physical adsorption is proposed to involve electrostatic attraction between protonated HBAT and chloride-covered regions of the steel surface. Chemical adsorption is proposed to involve electron donation from the O, N, and S atoms and the molecular π-system to iron d-orbitals. The resulting film is consistent with a reduction in available reaction sites and with restricted transport of aggressive ions. Gravimetric, EIS, and SEM results confirm that adsorption occurs and that a protective film forms; they do not by themselves distinguish physisorption from chemisorption or identify specific surface bonds.

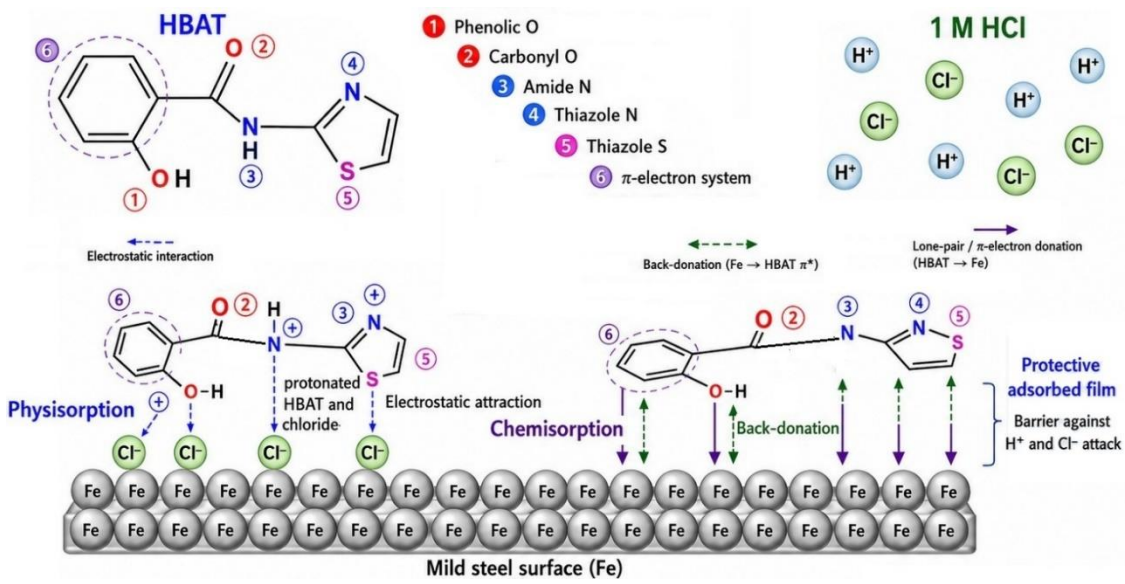


Figure 9: Proposed inhibition mechanism of HBAT on mild steel in 1 M HCl, illustrating electrostatic physisorption of protonated HBAT on the chloride-covered surface, proposed donor–acceptor chemisorption involving the O, N, and S atoms and the molecular π-electron system, and formation of a protective adsorbed film that suppresses anodic iron dissolution and cathodic hydrogen evolution.

4. Comparison with published corrosion inhibitors and significance of HBAT

To evaluate the significance of the present results, the corrosion-inhibition performance of HBAT was compared with representative nitrogen-, sulfur-, and oxygen-containing heterocyclic inhibitors reported for steel in hydrochloric acid. The comparison is presented in Table 5. Such comparisons should be interpreted cautiously because inhibition efficiency depends not only on molecular structure but also on inhibitor concentration, steel composition, acid concentration, temperature, immersion period, surface preparation, hydrodynamic conditions, and the experimental technique used to calculate the efficiency. Accordingly, Table 5 is intended to establish the performance context of HBAT rather than to provide an absolute ranking of corrosion inhibitors.

Table 5: Comparison of HBAT with representative heterocyclic corrosion inhibitors reported for steel in acidic media.

Inhibitor	Substrate / corrosive medium	Concentration	Principal conditions/method	Reported IE (%)	Comparative observation	Ref.
HBAT	Mild steel / 1 M HCl	0.5 mM	WL, 303 K, 5 h	94.82	High protection at low concentration	This work
HBAT	Mild steel / 1 M HCl	0.5 mM	WL, 303 K, 24 h	96.82	Protection increased during the first 24 h	This work
HBAT	Mild steel / 1 M HCl	0.5 mM	WL, 303 K, 48 h	96.81	Essentially unchanged from 24 to 48 h	This work
HBAT	Mild steel / 1 M HCl	0.5 mM	WL, 333 K, 5 h	96.65	Protection remained high and increased with temperature	This work
HBAT	Mild steel / 1 M HCl	0.5 mM	EIS, 303 K	94.91	(R_{ct}) increased from 47.53 to 933.25 Ω cm²	This work
Isatin–Schiff base, OHMHI	Mild steel / 1 M HCl	0.5 mM	WL, 303-333 K	96.1 at 303 K	Similar initial efficiency, but decreased to 85.5% at 333 K	[22]
Tris-thiosemicarbazone derivative, PMBMH	Mild steel / HCl	800 ppm	Electrochemical, 303 K	98.5	Higher initial value, but protection decreased with temperature and showed some deterioration with prolonged exposure	[23]
Benzoxazole-2-thione	C38 steel / 1 M HCl	0.1 mM	EIS	94.68	Excellent concentration efficiency; direct comparison is limited by differences in steel and electrochemical model	[38]
2-Amino-6-methylbenzothiazole (AMBT)	S235 steel / 1 M HCl	5 mM	WL/electrochemical, 298 K	83.30	Considerably lower efficiency despite a tenfold higher concentration	[39]
5-Amino-1,3,4-thiadiazole-2-thiol	Steel / HCl	Highest tested concentration	WL/electrochemical, 303–333 K	~81	Lower protection; adsorption followed Langmuir behavior	[41]
Triazole derivative, DTE	Mild steel / 1 M HCl	1.0 mM	WL/electrochemical, 298 K	>90.9	Lower maximum protection at twice the HBAT concentration	[42]
Aminotriazole, m-DTAT	Mild steel / HCl	0.4 mM	WL/electrochemical, 303 K	~95	Performance comparable with HBAT near ambient temperature	[43]

Table 5: Continue.

Inhibitor	Substrate / corrosive medium	Concentration	Principal conditions/method	Reported IE (%)	Comparative observation	Ref.
4-MTHT	Mild steel / HCl	0.5 mM	WL/electrochemical	99.6	Higher absolute efficiency and a strong benchmark for heterocyclic inhibitors	[44]
2-Amino-4-methylthiazole (2A4MT)	Mild steel / 0.5 M HCl	0.5 mM	EIS/LPR	92	HBAT gives higher EIS efficiency at the same concentration in a more concentrated HCl medium	[45]
2-Amino-4-methylthiazole (2A4MT)	Mild steel / 0.5 M HCl	5–10 mM	EIS/LPR	97–98	Comparable maximum protection required a substantially higher inhibitor concentration	[45]
Laurhydrazide N′-propan-3-one (LHP)	Mild steel / 5 M HCl	0.370 mM	PDP, 20 °C	94	Strong inhibitor in concentrated acid, but efficiency decreased strongly as temperature increased	[46]
5-Aminoindazole (AIA)	Q235 carbon steel / 1 M HCl	2.0 mM	EIS, 298 K	92.3	HBAT provides higher protection at one-quarter of this concentration	[47]
2-Aminothiazole (AT)	45# steel / 0.1 M HCl	500 mg L^{-1}	EIS/WL, 298 K	90.34	Lower efficiency in a less concentrated HCl medium	[48]
AAEE thiazole derivative	Mild steel / 1 M HCl	0.5 mM	WL, 303 K	93.3	Structurally related thiazole; HBAT provides greater efficiency at the same concentration	[49]
AAEE thiazole derivative	Mild steel / 1 M HCl	1.0 mM	WL, 303 K	96.1	Comparable efficiency requires approximately twice the HBAT concentration	[49]

The comparison demonstrates that HBAT belongs to the high-performance group of heterocyclic inhibitors for steel in hydrochloric acid. At 0.5 mM and 303 K, HBAT provided a gravimetric inhibition efficiency of 94.82 % after only 5 h and 96.82 % after 24 h. Importantly, extending the exposure to 48 h produced an efficiency of 96.81 %, indicating that the protection obtained after 24 h was essentially maintained during the subsequent 24 h. Thus, HBAT combines rapid initial inhibition with persistent protection during prolonged immersion. An important advantage of HBAT becomes apparent when the inhibitors are compared on a concentration basis. The structurally related AMBT produced only 83.30 % inhibition at 5 mM in 1 M HCl [39], whereas HBAT exceeded 94 % at only 0.5 mM. Similarly, 5-aminoindazole required 2 mM to obtain an EIS efficiency of approximately 92.3 % [47]. The simpler 2-amino-4-methylthiazole produced an EIS inhibition efficiency of approximately 92 % at 0.5 mM in 0.5 M HCl and required concentrations of 5-10 mM to approach 97-98 % according to impedance and polarization-resistance measurements [45]. In comparison, HBAT reached 94.91 % by EIS at 0.5 mM in the more aggressive 1 M HCl medium. Likewise, 2-aminothiazole reached a maximum efficiency of approximately 90.34 % at 500 mg L^{-1} in only 0.1 M HCl [48]. The additional experiment at 1.0 mM provides further evidence of the efficient utilization of HBAT. After 24 h, increasing the concentration from 0.5 to 1.0 mM increased the inhibition efficiency only from 96.82 to 96.94 %, corresponding to an improvement of only 0.12 percentage points despite doubling the inhibitor concentration. Thus, the corrosion-inhibition response approaches a plateau near 0.5 mM. This observation is important from a practical perspective because

increasing the amount of inhibitor beyond this level produces negligible additional protection under the investigated gravimetric conditions. The temperature response represents another favorable characteristic of HBAT. At 0.5 mM, the inhibition efficiency increased from 93.50 % at 303 K to 96.65 % at 333 K. This behavior differs from that of several reported organic inhibitors whose protective layers become less effective as the temperature increases. For example, OHMHI decreased from 96.1 % at 303 K to 85.5 % at 333 K [22]. AMBT also displayed a pronounced decline in protection with increasing temperature, from 81.93 % at 298 K to 66.30 % at 318 K at 5 mM [39]. LHP, although highly effective in the much more aggressive 5 M HCl medium, showed a decrease in polarization-derived inhibition efficiency from approximately 94 % at 20 °C to 73 % at 60 °C and 61 % at 80 °C [46]. These comparisons should not be treated as direct rankings because the acid concentrations and experimental conditions differ, but they emphasize the favorable thermal persistence of the HBAT film.

A useful comparison can also be made with the structurally related AAEE thiazole derivative. AAEE provided approximately 93.3 % inhibition at 0.5 mM and 303 K and approximately 96.1 % when its concentration was increased to 1.0 mM [49]. HBAT therefore provides slightly higher protection at the common concentration of 0.5 mM and reaches approximately the same efficiency range without requiring the inhibitor concentration to be doubled. Both compounds nevertheless demonstrate that combining a thiazole adsorption center with additional aromatic and oxygen-containing functionality is a productive strategy for enhancing adsorption on mild steel. DFT descriptors are consistent with donor sites on the thiazole–hydroxybenzamide framework; this does not prove structural superiority without those calculations. The thiazole moiety provides nitrogen and sulfur centers capable of interaction with surface iron, whereas the 2-hydroxybenzoyl unit introduces carbonyl and phenolic oxygen atoms together with an additional aromatic π-electron system. DFT descriptors are consistent with donor sites on the thiazole–hydroxybenzamide framework (N, S, carbonyl and phenolic O, and the aromatic π-system). A chemically reasonable hypothesis is that these additional centres contribute to the observed high efficiency of HBAT at 0.5 mM relative to simpler aminothiazole structures reported under different conditions. This hypothesis is not directly demonstrated by the present experiments and does not constitute an established explanation of superior performance, nor an absolute ranking of HBAT above the literature inhibitors in Table 5. The adsorption and EIS results provide additional support for this structure–performance interpretation. HBAT adsorption was best represented by the Langmuir relationship, with a slope close to unity and a high regression coefficient. At the same time, increasing the HBAT concentration to 0.5 mM increased the charge-transfer resistance from 47.53 to 933.25 Ω cm² and produced an EIS inhibition efficiency of 94.91 %. The simultaneous increase in charge-transfer resistance and decrease in effective double-layer capacitance indicate active-site blocking, displacement of interfacial water, and formation of a more resistive inhibitor-rich layer. The gravimetric, adsorption, EIS, and SEM observations therefore provide mutually consistent evidence for the development of an effective protective interfacial film. It should nevertheless be emphasized that HBAT does not exhibit the highest absolute inhibition efficiency ever reported. For example, 4-MTHT has reached approximately 99.6 % at 0.5 mM [44], and other inhibitors have also produced very high initial efficiencies under particular conditions. Benzo-xazole-2-thione additionally demonstrates excellent concentration efficiency, producing approximately 94.68 % by EIS at only 0.1 mM [38]. Consequently, the contribution of HBAT should not be based on an unsupported claim of record inhibition efficiency. Rather, the principal contribution of the present inhibitor lies in the combination of several favorable characteristics: (i) inhibition efficiencies approaching 97 % at only 0.5 mM, (ii) negligible benefit from doubling the concentration to 1.0 mM, demonstrating a practical concentration plateau, (iii) essentially unchanged protection between 24 and 48 h at 0.5 mM, (iv) retention and enhancement of corrosion protection up to 333 K, (v) strong Langmuir-type adsorption, and (vi) close agreement between gravimetric, electrochemical, and surface-morphology observations. Considered together, these properties make HBAT a highly efficient aminothiazole-based inhibitor under the investigated conditions and distinguish it from many simpler heterocyclic inhibitors for which high efficiency requires greater concentrations or decreases substantially with temperature.

5. Conclusions

HBAT inhibits the corrosion of mild steel in 1 M HCl under the investigated conditions. Gravimetric measurements show high inhibition efficiency at a relatively low concentration, a practical plateau near 0.5 mM, and persistent protection during prolonged immersion: at 0.5 mM and 303 K the efficiency increased from 93.50 % after 1 h to 96.82 % after 24 h and remained 96.81 % after 48 h. Doubling the concentration to 1.0 mM produced only a marginal further improvement. At 0.5 mM the gravimetric efficiency increased to 96.65 % at 333 K. EIS at 303 K showed an increase in charge-transfer resistance from 47.53 to 933.25 Ω cm^2 and a decrease in effective capacitance, corresponding to 94.91% inhibition at 0.5 mM. Adsorption was best described by the Langmuir isotherm. SEM showed reduced surface damage in the inhibited acid. A mixed physical and chemical adsorption mode is proposed, involving electrostatic interaction of protonated HBAT with chloride-covered regions of the surface and possible electron donation from N, S, O, and the aromatic π-system. FTIR and XPS of the adsorbed layer were not performed, so specific Fe-heteroatom bonds are not claimed. These experimental characteristics identify HBAT as a highly efficient aminothiazole-based inhibitor for mild steel in 1 M HCl under the conditions of this study. Techno-economic, toxicity, and long-term exposure assessments were outside the present scope.

Institutional contributions

This work was conducted independently under the affiliation of Al-Ayen Scientific Research Center, Al-Ayen Iraqi University, AUIQ, An Nasiriyah, Thi Qar, Iraq. The institution provided access to research materials and scholarly databases but had no influence on the study design, data interpretation, or publication process.

6. References

1. Li M, Liu F, Mou F, Guo Z, Wang W, Zeng Y, Sim LB, Chen B. Corrosion inhibitor for mild steel in mixed HCl and H_2SO_4 medium: A study of 1,10-phenanthroline derivatives. ACS Omega. 2025;10: 24628-24641. https://doi.org/10.1021/acsomega.5c01412.
2. Zaripova YF, Razhabov S, Pavelyev RS, Vinogradova SS, Nazmutdinov RR, Vakhitov IR, Varfolomeev MA. Effective inhibition of carbon steel corrosion by waterborne polyurethane based on N-tert-butyl diethanolamine in 2M HCl: Experimental and computational findings. Energies. 2022;15:1939. https://doi.org/10.3390/en15051939.
3. Azzouni D, Alaoui Mrani S, Bertani R, Alanazi MM, En-nabety G, Taleb M. Experimental and theoretical investigation of the inhibitor efficiency of Eucalyptus globulus leaf essential oil on mild steel corrosion in a molar hydrochloric acid medium. Molecules. 2024; 29:3323. https://doi.org/10.3390/molecules29143323.
4. Kadiri M, Driouch M, Elaaraj I, Tanji A, Elabbadi A, Fahim M, Sfaira M, Hermawan H. Synergistic corrosion inhibition of mild steel in acidic media by a benzimidazole-thiophene ligand and its metal complexes: A multi-technique electrochemical approach. Materials. 2025;18:4545. https://doi.org/10.3390/ma18194545.
5. Althobaiti IO, Eid S, El-Nasser KS, Hashem N, Salama EE. Evaluation of the impact of two thiadiazole derivatives on the dissolution behavior of mild steel in acidic environments. Molecules. 2023; 28:3872. https:// doi.org/10.3390/molecules28093872.
6. Sehmi A, Boudou F, Bouchikhi N, Ait Amer A, Zaoui F, Zebida M, Benali O, Lasri B, Gherdaoui CE. Isoxazole-based corrosion inhibitor for mild steel in acidic medium: Adsorption, electrochemical, and computational studies. Disc Chem. 2026;3:222. https://doi.org/10.1007/s44371-026-00644-2.
7. Hanoon MM, Resen AM, Shaker LM, Kadhum AAH, Al-Amiery AA. Corrosion investigation of mild steel in aqueous hydrochloric acid environment using N-(naphthalen-1-yl)-1-(4-pyridinyl)methanimine complemented with antibacterial studies. Biointerface Res Appl Chem. 2021;11(2):9735-9743. https://doi.org/10.33263/BRIAC112.97359743.
8. Fouda AS, Elmorsi MA, Fayed T, El Said IA. Oxazole derivatives as corrosion inhibitors for 316L stainless steel in sulfamic acid solutions. Desalin Water Treat. 2016;57:4371-4385. https://doi.org/10.1080/19443994.2014.9937 17.
9. Guo L, Obot IB, Zheng X, Shen X, Qiang Y, Kaya S, Kaya C. Theoretical insight into an empirical rule about organic corrosion inhibitors containing nitrogen, oxygen, and sulfur atoms. Appl Surf Sci. 2017;406: 301-306. https://doi.org/10.1016/j.apsusc.2017.02.134
10. Popova A, Christov M. Evaluation of impedance measurements on mild steel corrosion in acid media in the presence of heterocyclic compounds. Corr Sci. 2006; 48:3208-3221. https://doi.org/10.1016/j.corsci.2005.11.001.
11. Singh AK, Quraishi MA. The effect of some bis-

thiadiazole derivatives on the corrosion of mild steel in hydrochloric acid. Corr Sci. 2010; 52:1373-1385. https://doi.org/10.1016/j.corsci.2010.01.007.
12. Loto RT, Loto CA, Popoola AP. Corrosion inhibition of thiourea and thiadiazole derivatives: a review. J Mater Environ Sci. 2012; 3(5):885-894.
13. Ammal PR, Prajila M, Joseph A. Effective inhibition of mild steel corrosion in hydrochloric acid using EBIMOT, a 1,3,4-oxadiazole derivative bearing a 2-ethylbenzimidazole moiety: Electroanalytical, computational and kinetic studies. Egyptian J Petroleum. 2018; 27:823-833. https://doi.org/10.1016/j.ejpe.2017.12.004.
14. Afzalkhah M, Masoum S, Behpour M, Naeimi H, Reisi-Vanani A. Experimental and theoretical investigation of inhibition efficiency of 2-(2-hydroxyphenyl)-benzothiazole using impedance spectroscopy, experimental design, and quantum chemical calculations. Indust Eng Chem Res. 2017;56:9035-9044. https://doi.org/10.1021/acs.iecr.7b02030.
15. Kosari A, Moayed MH, Davoodi A, Parvizi R, Momeni M, Eshghi H, Moradi H. Electrochemical and quantum chemical assessment of two organic compounds from pyridine derivatives as corrosion inhibitors for mild steel in HCl solution under stagnant condition and hydrodynamic flow. Corr Sci. 2014; 78: 138-150. https://doi.org/10.1016/j.corsci.2013.09.009.
16. ASTM G 31-72, Standard Guide for Laboratory Immersion Corrosion Testing of Metals. American Society for Testing and Materials: Philadelphia, PA, USA, 1990.
17. TM0169/G31-12a, Standard Guide for Laboratory Immersion Corrosion Testing of Metals. NACE International: Houston, TX, USA, 2012.
18. Talat R, Asghar MA, Tariq I, Akhter Z, Liaqat F, Nadeem L, Haider A, Ali S. Evaluating the Corrosion Inhibition Efficiency of Pyridinium-Based Cationic Surfactants for EN3B Mild Steel in Acidic-Chloride Media. Coatings. 2022;12:1701. https://doi.org/10.3390/coatings12111701.
19. Nataraja SE, Venkatesha TV, Manjunatha K, Poojary B, Pavithra MK, Tandon HC. Inhibition of the corrosion of steel in hydrochloric acid solution by some organic molecules containing the methylthiophenyl moiety. Corr Sci. 2011;53:2651-2659. https://doi.org/10.1016/j.corsci.2011.05.004.
20. Abd El Rehim SS, Sayyah SM, El-Deeb MM, Kamal SM, Azooz RE. Adsorption and corrosion inhibitive properties of P(2-aminobenzothiazole) on mild steel in hydrochloric acid media. Inter J Indust Chem. 2016; 7:39-52. https://doi.org/10.1007/s40090-015-0065-5.
21. Yuan Z, Du Q, Zhou Z, Zou Y, Kang J, Liao X, Hou D, Jiang H, Xiong W. Sustainable corrosion inhibitors from Furil: structure-performance relationship and adsorption mechanism via experimental and theoretical studies. Appl Surf Sci. 2026; 736:166811. https://doi.org/10.1016/j.apsusc.2026.166811.
22. Al-Amiery AA, Betti N, Isahak WNRW, Al-Azzawi WK, Wan Nik WMN. Exploring the effectiveness of isatin-Schiff base as an environmentally friendly corrosion inhibitor for mild steel in hydrochloric acid. Lubricants. 2023;11:211. https://doi.org/10.3390/lubricants11050211.
23. Abuelela AM, Bedair MA, Gad ES. Exploring the synthesis, characterization, and corrosion inhibition of new tris-thiosemicarbazone derivatives for acidic steel settings using computational and experimental studies. Sci Rep. 2024;14:13310. https://doi.org/10.1038/s41598-024-64199-x.
24. Chaouiki A, Chafiq M, Ko YG, Al-Moubaraki AH, Thari FZ, Salghi R, Karrouchi K, Bougrin K, Ali IH, Lgaz H. Adsorption mechanism of eco-friendly corrosion inhibitors for exceptional corrosion protection of carbon steel: electrochemical and first-principles DFT evaluations. Metals. 2022;12:1598. https://doi.org/10.3390/met12101598.
25. Dima GD, Dan ML, Rudenko N, Vaszilcsin N. Evaluation of the inhibitory efficiency of yohimbine on corrosion of OLC52 carbon steel and aluminum in acidic acetic/acetate media. Coatings. 2025; 15:1458. https://doi.org/10.3390/coatings15121458.
26. Resen AM, Hanoon M, Salim RD, Al-Amiery AA, Shaker LM, Kadhum AAH. Gravimetrical, theoretical, and surface morphological investigations of corrosion inhibition effect of 4-(benzoimidazole-2-yl) pyridine on mild steel in hydrochloric acid. Koroze Ochr Mater. 2020;64(4):122-130. https://doi.org/10.2478/kom-2020-0018.
27. Xu Y, Gao Y, Wang J, Zhang K, Zhang Y, Yang W, Aslam R, Wang Q. Lotus (nelumbo nucifera gaertn.) leaf extract as a green corrosion inhibitor for copper in sulfuric acid media. Coatings. 2026;16:501. https://doi.org/10.3390/coatings16040501.
28. Wang Y, Wang P, Li J, Wang S, Li W, Li C. Insight into anti-corrosion behavior and mechanism of 8-hydroxyquinoline inhibitor on AZ91D alloy in different concentrations of sodium chloride solution. Coatings. 2023;13:1595. https://doi.org/10.3390/ coatings13091595.
29. Răuță, D.-I., Brânzoi, F., Avramescu SM, Truşcă, R.-D., Matei E. Eco-friendly corrosion inhibition of OLC45 steel in H_2SO_4 solution using rhus typhina L. Plant Extract Technol. 2026;14:256. https://doi.org/10.3390/technologies14050256.
30. Lazanas AC, Prodromidis MI. Electrochemical impedance spectroscopy-A tutorial. ACS Measure-ment Sci. 2023;3(3):162-193. https://doi.org/10.1021/acsmeasuresciau.2c00070.
31. Hu S, Li S, Wen J, Yuan X, Li F. Effect of Ni on the natural passivating film and pitting corrosion resistance of stainless steels in alkaline media. Coatings. 2026; 16(1):81. https://doi.org/10.3390/coatings16010081.
32. Kamboj V, Bhushan B, Kumar Singh M, Nayak A, Rastogi C, Mangla B, Ji G. Investigation on the working mechanisms of sustainable corrosion inhibitors for mild steel in acid solutions: a review based on experimental and computational analysis. Surf Sci Technol. 2026;4(1):13. https://doi.org/10.1007/s44251

- 025-00119-z.
33. Fekry AM, Ameer MA. Corrosion inhibition of mild steel in acidic media using newly synthesized heterocyclic organic molecules. Inter J Hydrogen Energy. 2010;35(14):7641-51. https://doi.org/10.1016/ j. ijhydene.2010.04.111.
34. El-khlifi A, Lgaz H, Safi Z, Wazzan N. Molecular-level insights into corrosion inhibition efficiency of semicarbazone derivatives on carbon steel: a synergistic DFT and DFTB. Invest Surf Inter Anal. 2026. https://doi.org/10.1002/sia.70088.
35. Wazzan S, Safi Z, Wazzan N. Unveiling the electronic and thermodynamic properties of 2-furaldehyde semicarbazone derivatives: combined DFT and M-polynomial topological indices analysis. Sci Report. 2026; 16:24284. https://doi.org/10.1038/s41598-026-50777-8.
36. Rajanna BR, Sadhana V, Veda T, Gosu NR, Ashok Reddy GV, Kumar KN, G H. Anti-corrosive behavior of nitro-engineered 1,3,4-thiadiazoles for mild steel C-1030: a comprehensive potentiodynamic study. Mater Corr. 2026. https://doi.org/10.1002/maco.70217.
37. Morchid Elidrissi Z, Mouloudi M, Essahli M, Chhiba M. Experimental investigation of corrosion inhibitor performance for carbon steel in industrial hydrochloric acid pickling. Eng. 2026;7:288. https://doi.org/10. 3390/ eng7060288.
38. Omari M, Bouiti K, Jebbari S, Lahrache N, Barhoumi A, Labjar N, Hajjaji SE, Said-Ahmed M, Lebrini M, Nasrellah H, et al. Corrosion inhibition of C38 steel in 1 M HCl using benzoxazole-2-thione: electro-chemical, SEM-EDX, and theoretical studies. Metals. 2025; 15:810. https://doi.org/10.3390/met15070810.
39. Xhanari K, Farruku M, Berisha A, Seiti B, Xhaxhiu K, Kokalari E, Lame A. 2-Amino-6-methylbenzothiazole as corrosion inhibitor for low carbon steel in acidic solution: experimental and theoretical studies. Result Chem. 2025; 13:101922. https://doi.org/10.1016/j. rechem.2024.101922.
40. Deng Q, Jeschke S, Mishra RK, Spicher S, Darouich S, Schreiner E, Eiden P, Deglmann P, Gorges JN, Chen XB, Keil P. Design of alkyl-substituted aminothiazoles to optimise corrosion inhibition for galvanised steel: A combined experimental and molecular modelling approach. Corr Sci. 2024; 227: 111733. https://doi.org/10.1016/j.corsci.2023.111733
41. Helmy M, El-Zomrawy AA, Mogoda AS, Nasser A, Mahmoud M, Mohamed TA. Corrosion inhibition of ductile iron in hydrochloric acid using 5-amino-1, 3, 4-thiadiazole-2-thiol: electrochemical and compu-tational studies. Sci Reports. 2026; 16(1):14740. https://doi.org/10.1038/s41598-026-51250-2.
42. Xu F, Duan J, Zhang S, Hou B. The inhibition of mild steel corrosion in 1 M hydrochloric acid solutions by a triazole derivative. Mater Lett. 2008; 62:4072-4074. https://doi.org/10.1016/j.matlet.2008.05.037.
43. El Mehdi B, Mernari B, Traisnel M, Bentiss F, Lagrenée, M. Synthesis and comparative study of the inhibitive effect of some new triazole derivatives towards corrosion of mild steel in hydrochloric acid solution. Mater Chem Phys. 2003; 77:489-496. https://doi.org/10.1016/S0254-0584(02)00085-8.
44. Bentiss F, Bouanis M, Mernari B, Traisnel M, Vezin H, Lagrenée, M. Understanding the adsorption of 4H-1,2,4-triazole derivatives on mild steel surface in molar hydrochloric acid. Appl Surf Sci. 2007;253: 3696-3704. https://doi.org/10.1016/j.apsusc.2006.08. 001.
45. Yüce, A.O., Mert BD, Kardaş, G., Yazıcı B. Electrochemical and quantum chemical studies of 2-amino-4-methyl-thiazole as corrosion inhibitor for mild steel in HCl solution. Corr Sci. 2014; 83:310-316. https://doi.org/10.1016/j.corsci.2014.02.029.
46. El-Haddad MAM, Radwan AB, Sliem MH, Hassan WMI, Abdullah AM. Highly efficient eco-friendly corrosion inhibitor for mild steel in 5 M HCl at elevated temperatures: experimental & molecular dynamics study. Sci Rep. 2019;9:3695. https://doi.org/ 10.1038/s41598-019-40149-w.
47. Xu S, Zhang S, Guo L, Feng L, Tan B. Experimental and theoretical studies on the corrosion inhibition of carbon steel by two indazole derivatives in HCl medium. Materials. 2019;12:1339. https://doi.org/ 10.3390/ma12081339.
48. Cui FY, Guo L, Zhang S-T. Experimental and theoretical studies of 2-amino thiazole as an inhibitor for carbon steel corrosion in hydrochloric acid. Mater Corr. 2014;65(12):1194-1201. https://doi.org/10.1002/ maco.201307591.
49. Khalaf MM, Sultan AE, Hussein FH, et al. Corrosion inhibition of mild steel in corrosive solution by 2-amino-4-(4-methoxyphenyl)thiazole-5-carboxylic acid ethyl ester: Experimental and DFT investigations. Int J Corros Scale Inhib. 2024;13:2400-2423. https://doi. org/10.17675/2305-6894-2024-13-4-28.
50. Farahati R, Ghaffarinejad A, Mousavi-Khoshdel SM, et al. Synthesis and potential applications of some thiazoles as corrosion inhibitor of copper in 1 M HCl: Experimental and theoretical studies. Prog Org Coat. 2019; 132:417-428. https://doi.org/10.1016/j.porgcoat. 2019.04.005.
51. Scaria PT, Shetty P, Kumari PP, Kagatikar S 2-Aminobenzothiazole as an efficient corrosion inhibitor of AA6061-T6 in 0.5 M HCl medium: electro-chemical, surface morphological, and theoretical study. J Appl Electrochem. 2022; 52:1675-1689. https://doi.org/10.1007/s10800-022-01742-6.

How to cite this article:
Khalid Ahmed R, Saad Azeez H, Halbos RJ, Amir H. Kadhum A, Al-Amiery A. HBAT as a High-Efficiency Corrosion Inhibitor for Mild Steel in 1 M HCl: Gravimetric, Electrochemical, Adsorption, and Surface Studies. Prog Color Colorants Coat. 2027;20(3):367-389. https://doi.org/10.30509/ pccc.2026.167849.1528.

